HHS Public Access

Author manuscript

Metallomics. Author manuscript; available in PMC 2015 September 01.

Published in final edited form as:

Metallomics. 2014 September ; 6(9): 1664–1670. doi:10.1039/c4mt00099d.

Kinetic Results for Mutations of Conserved Residues H304 and R309 of Human Sulfite Oxidase Point to Mechanistic Complexities

Amanda C. Davis[1], **Kayunta Johnson-Winters**[2,*], **Anna R. Arnold**[1], **Gordon Tollin**[1], and **John H. Enemark**[1]

[1]Department of Chemistry and Biochemistry, University of Arizona, Tucson, Arizona, 85721-0041

[2]Department of Chemistry and Biochemistry, University of Texas at Arlington, Arlington, Texas 76019-0065

Abstract

Several point mutations in the gene of human sulfite oxidase (hSO) result in isolated sulfite oxidase deficiency, an inherited metabolic disorder. Three conserved residues (H304, R309, K322) are hydrogen bonded to the phosphate group of the molybdenum cofactor, and the R309H and K322R mutations are responsible for isolated sulfite oxidase deficiency. The kinetic effects of the K322R mutation have been previously reported (Rajapakshe et al. 2012, *Chem. Biodiversity 9*, 1621-1634); here we investigate several mutants of H304 and R309 by steady-state kinetics, laser flash photolysis studies of intramolecular electron transfer (IET), and spectroelectrochemistry. An unexpected result is that all of the mutants show *decreased* rates of IET but *increased* steady-state rates of catalysis. However, in all cases the rate of IET is greater than the overall turnover rate, showing that IET is not the rate determining step for any of the mutations.

Introduction

Sulfite oxidizing enzymes are molybdenum-containing enzymes that occur in animals, plants and bacteria. In animals, sulfite oxidase (SO) is a molybdoheme enzyme that is located in the intermembrane space of the mitochondria and is essential for oxidizing toxic sulfite to sulfate, which can then be excreted (eq. 1). The proposed catalytic cycle for human sulfite oxidase (hSO) is shown in Figure 1. Regeneration of the enzyme includes two, one-electron *intramolecular* electron transfers (IET) from the molybdenum (Mo) to the heme Fe and two, one-electron *intermolecular* electron transfers from the Fe to external ferricytochrome *c* (1-5).

$$SO_3{}^{2-} + \mathrm{H_2O} + 2(cyt\quad c)_{ox} \rightarrow SO_4{}^{2-} + 2(cyt\quad c)_{red} + 2\mathrm{H}^+ \quad (1)$$

In humans, sulfite oxidase deficiency is an inherited metabolic disorder that leads to severe neonatal neurological defects and early death (6). The inability to biosynthesize the

*Kayunta@uta.edu.

molybdenum cofactor (Moco, Figure 2) results in “general sulfite oxidase deficiency”, which compromises all molybdenum enzymes (7). However, recent determination of the biosynthetic pathway of Moco has made possible the first clinical treatment of “general SO deficiency” (8). Several point mutations in the hSO gene also result in sulfite oxidase deficiency (9, 10). Our research has focused on investigating the effects of such point mutations on the structure, solution dynamics, and the catalytic mechanism of hSO with the long-term goal that understanding “isolated sulfite oxidase deficiency” at the molecular level may eventually lead to treatment protocols for this condition.

No crystal structure is available for hSO, so the crystal structure of the highly homologous chicken sulfite oxidase (cSO), shown in Figure 3, is used as a structural template for hSO (11). The crystal structure of cSO shows that the enzyme is a homodimer and that each monomer is made up of a molybdenum cofactor (Moco) containing domain and a smaller, cytochrome b_5-type domain (heme domain). These two domains are linked by a flexible polypeptide tether with no secondary structure (11). In the crystal structure and in frozen solution (12) the Mo···Fe distance is ~32 Å. However, it is proposed that in fluid solution the tether allows the heme domain to move within close proximity to the Mo center so that rapid IET and efficient catalysis can occur (12-16).

Previous studies of hSO mutants have shown a range of interesting properties and reactivities, some of which were quite unexpected. These mutations include: deletion of tether residues (17); mutation of the aromatic residues around both the heme and Mo domains (18, 19); mutation of conserved active site residues (20-22); and producing some of the fatal mutations (22-26) such as R160Q and K322R. Although many of these mutants have provided much insight into the structural and kinetic characteristics of hSO, some have shown unexplained or even paradoxical results. For example, mutation of H337 and W338 on the surface of the Mo domain influence the potential of the heme domain, despite the large distance between these residues and the heme in the crystal structure (18). Mutations such as K322R, W338A, H337R, and ΔKVATV, show IET rates that are much less than wt hSO and sometimes less their own k_{cat} values, while k_{cat} in many cases has *increased* significantly as compared to wt (17, 18, 25). These results illustrate the complexity of hSO and indicate that the roles of conformational change and other factors in the catalytic cycle and IET reactions of hSO and their relationship to isolated sulfite oxidase deficiency are yet to be understood.

The phosphate group of the molybdenum cofactor is associated with three conserved, positively charged residues, H304, R309, and K322, that hydrogen bond to one another and to the negatively charged phosphate group (Figure 2) (11). Two of these residues, R309H and K322R, have been linked to isolated sulfite oxidase deficiency (10). A study of the K322R mutant has been recently described (25); the present study focuses on histidine 304 (H304) and arginine 309 (R309). H304 is located on the surface of the Mo domain and is hydrogen bonded to R309 and to the phosphate group of Moco. R309 is located just under the surface of the Mo domain and hydrogen bonds to the phosphate of Moco, H304, and K322 (11). In the present study, several mutations of H304 and R309 have been prepared and purified, and the recombinant enzymes have been characterized using steady-state kinetics, laser flash photolysis, and spectroelectrochemistry. The unexpected results that

were obtained for the H304 and R309 mutants are compared to the other classes of hSO mutants described above, and the challenges of developing a comprehensive molecular mechanism for catalysis by hSO are discussed.

Experimental

Site-directed mutagenesis

The mutations were introduced into the pTG918 plasmid containing the wt hSO sequence using the Quick Change Site-Directed Mutagenesis protocol (Stratagene) (27). The Sequetech Corporation DNA analysis facility in Mountain View, California confirmed each of the single amino acid mutations by DNA sequence analysis (see supporting information, Table S1).

Protein over-expression and purification

The recombinant hSO mutants were introduced into *E. coli* and purified using a previously established method for hSO proteins with the following modifications (27, 28). After the DE-52 column (GE Healthcare), the fractions with an A_{413}/A_{280} ratio of 0.80 or greater were collected and purified further through a Phenyl Sepharose column (GE Healthcare). The fractions that had an A_{413}/A_{280} ratio of 0.95 or greater were then purified using a Superdex 200 column (GE Healthcare). The enzyme concentration was calculated by using the molar extinction coefficient of 113,000 M^{-1} cm^{-1} at 413 nm (20). The Mo:Fe ratio of each purified protein was determined using an IRIS Advantage Inductively Coupled Plasma Emission Spectrometer (*ICP-OES*) from the Jarrell Ash Corporation (see supporting information, Table S2).

Steady-state kinetics

Steady-state kinetics studies were performed aerobically at 25°C using a Varian Cary-300 spectrophotometer. Initial velocities were calculated following the reduction of freshly prepared oxidized cyt *c* (horse heart, Sigma) at 550 nm (ε = 19, 630 M^{-1} cm^{-1}) (29). Samples were prepared using 20 mM Tris buffer, adjusted to pH 7.6 using acetic acid. 20 mM Bis-Tris was used for samples for which the pH was adjusted to 6.8 using acetic acid. The kinetic profile for obtaining the Michaelis-Menten constant, K_m, for sulfite and k_{cat}, for the reduction of cyt *c*, was studied using a saturating concentration of cyt *c* (400 μM; 10-fold greater than $K_m{}^{cyt\ c}$ for wt hSO) and by varying the concentration of sulfite between 1 μM and 400 μM. The concentration of enzyme was 50 nM. A sample kinetic profile is shown in the Supporting Information. Since k_{cat} is defined as per cyt *c* reduced (29) and two cyt *c* are reduced per turnover cycle (Figure 1), $k_{turnover}$ = ½ k_{cat}. Table S3 summarizes the kinetic parameters for wt hSO and each of the mutants.

Laser flash photolysis

IET 2 (Figure 1) in the hSO catalytic cycle can be studied using a photochemical one-electron reduction of the Fe(III) state and following its re-oxidation by Mo(VI) (30). Laser flash photolysis experiments of the mutants were done anaerobically using 300 μL of solution containing ~90 μM 5-deazariboflavin (dRF), 0.5 mM freshly prepared semicarbazide (the sacrificial reductant) and enzyme concentrations of 10 μM, 15 μM, and

20 μM. The methodologies for determining equilibrium constants and rate constants for hSO using this technique have been described previously (13). The laser flash system (31) and the process by which the enzyme sample is photochemically reduced have also been previously described (32-34) and are summarized below (eqs. 2-5).

$$dRF \rightarrow {}^{3}dRF \quad (2)$$

$${}^{3}dRF + AH_2 \rightarrow dRFH^{*} + AH^{*} \quad (3)$$

$$dRFH^{*} + Mo^{VI}Fe^{III} \rightarrow dRF + Mo^{VI}Fe^{II} \quad (4)$$

$$Mo^{VI}Fe^{II} \underset{k_r}{\overset{k_f}{\rightleftharpoons}} Mo^{V}Fe^{III} \quad (5)$$

By fitting the heme re-oxidation curve with an exponential function, the IET rate constant, k_{et}, can be calculated (eq. 6). The IET rate constant (k_{et}) is the sum of the forward (k_f) and the reverse (k_r) electron transfer rate constants (eq. 7). The parameters *a* and *b* are determined from kinetic traces and can be used to calculate the equilibrium constant (eqs. 8-10). Note that the direction of IET in the laser flash photolysis experiments is actually the reverse of the net physiological catalytic reaction (Figure 1).

$$\mathrm{d}A_{555}/\mathrm{d}t = a + b\,exp\,(-k_{et}t) \quad (6)$$

$$k_{et} = k_f + k_r \quad (7)$$

$$a = \mathrm{A}_0\,(k_r/k_{et})$$

$$b = \mathrm{A}_0\,(k_f/k_{et}) \quad (9)$$

$$K_{eq} = k_f/k_r = b/a \quad (10)$$

Spectroelectrochemistry

Spectroelectrochemical measurements of the heme reduction potentials were determined using the same type of instrumentation and reference electrode as described previously (35, 36). A spectroelectrochemical cell, gold working electrode, and platinum wire auxiliary electrode (BASi) were used to hold a 400 μL sample. Protein samples were prepared in 20 mM Tris buffer, pH 7.4, containing two electrochemical mediators, hexaammineruthenium chloride and anthraquinone 2-sulfonate (purchased from Aldrich) (37). Protein concentration ranged from 300 μM to 400 μM.

Since the wavelength dependences of the extinction coefficients of the reduced and oxidized forms of hSO differ from one another, the ratio of the oxidized to reduced forms is directly related to the absorbances of the optical spectra via Beer's law, and the change in absorbance with respect to the applied potential can be fit to the Nernst equation (Eq. 11) using the nonlinear-least-squares fitting algorithm in the software program Origin©:

$$E_{app}=E^{0}+2.303\,(RT/nF)\,log_{10}\,([Ox]\,/\,[Red]) \quad (11)$$

where E_{app} is the applied potential, E_0 is the midpoint potential determined from these data, and [Ox] and [Red] are, respectively, the concentrations of the Fe(III) and Fe(II) states of the b_5 heme of hSO. For a previous application of this method to hSO see Figure 4 of ref 17.

Results and discussion

Steady-state kinetics

The diversity of amino acids in the eight various mutations of H304 and R309 described herein involve replacing the histidine or arginine with a residue of different charge or of a drastically different size. All of the H304 and R309 mutations had *greater* catalytic activity than wt hSO. For H304A and H304E, k_{cat} was doubled compared to wt hSO, and all of the other mutant enzymes were three to four times as fast as wt hSO. Surprisingly, R309E, a mutation in which a positively charged residue is changed to a negatively charged residue, showed the highest k_{cat} of all the mutants. The increases in k_{cat} for all the mutants, rather than significant decreases, were unexpected given the hydrogen bonding interactions of H304 and R309 with the phosphate group of the molybdenum cofactor and the proximity of these residues to the active site of the enzyme. On the other hand, the fact that H304 and R309 are conserved across all eukaryotic sulfite oxidases suggests that their primary role may be anchoring or stabilizing Moco through hydrogen bonding rather than optimizing catalytic activity. Crystal structures of appropriate mutants of H304 and R309 are required to test this hypothesis.

The $K_m^{sulfite}$ values for the H304 and R309 mutant enzymes were not drastically altered from wt hSO, despite the fact that H304 and R309 are located within relatively close proximity to the Mo active site. H304F, H304E, R309K, and R309M showed K_m values similar to wt, whereas H304R, R309H, and the double mutant version of the two, H304R/R309H, showed slight increases in $K_m^{sulfite}$. R309E, which showed the greatest increase in activity, also showed the greatest increase in K_m. So although this mutation caused the enzyme to catalyze the oxidation of sulfite to sulfate much more quickly than wt, it did not bind sulfite as efficiently as wt hSO. Lastly, H304A, a mutation that removes the charge, hydrogen bonding, and is of smaller size, showed a decrease in $K_m^{sulfite}$, thus binding sulfite more efficiently than wt. Again, k_{cat} was increased compared to wt.

Intramolecular electron transfer (IET)

All of the R309 mutations caused large decreases in the k_{et} value for IET that were pH dependent (Figure 5B). R309K showed the least change, and R309E showed the most change. This makes sense in that mutating the arginine to lysine (R309K) keeps the positive charge and has the most comparable size to wt of all the mutations. Mutating the arginine to

glutamate (R309E) changes the charge from positive to negative while reducing the size of the residue. The result for R309E is also consistent with the proposal that the rate-limiting step of IET is a docking process, in which the negatively charged heme domain interacts with the positively charged Mo domain (38). Decreasing the positive charge of the Mo domain by the R309E mutation should decrease the electrostatic attraction between the two domains and thereby decrease the IET rate.

At pH 7.6 and 6.8, the IET rates of R309K, R309H, and R309M were approximately half that of wt hSO (Figure 5B). For all three of these mutants, $k_{et} > ½\ k_{cat} = k_{turnover}$, indicating that IET 2 is not the rate determining step. At pH 7.6, R309E showed the smallest k_{et} (67 s^{-1}) of the R309 mutants, but even this mutant with reversed charges had k_{et} slightly larger than $k_{turnover}$ (63 s^{-1}, Table S3). At pH 6.8 R309E did not show any reoxidation of the Fe(II).

The IET rates of the H304 mutants are shown in Figure 5A. At pH 7.4, the IET rates of H304A, H304F, and H304R/R309H were less than half as fast as wt, and H304E and H304R were about 100 s^{-1} slower than wt hSO. At pH 6.8, all mutant enzymes had IET rates that were two to three times less than that of wt hSO, with H304F being the most affected.

It is interesting to note that the IET rates *decreased* significantly, while the rates of catalysis *increased* considerably. This apparent discrepancy has previously been explained for other hSO mutants by the possible differences in the enzyme starting conformations that are probed by the steady-state kinetics and laser flash photolysis experiments (18). During steady-state kinetics, the proposed first step (Figure 1) is the binding of sulfite and a two-electron reduction of the Mo(VI)/Fe(III) resting state species to Mo(IV)/Fe(III). The first IET reaction (IET 1, Figure 1) converts Mo(IV)/Fe(III) to Mo(V)/Fe(II). This results in the appearance of a Mo(V) EPR signal and is known to occur in all hSO mutants, even the fatal R160Q mutant (24). From previous microcoulometry studies of cSO, the IET 1 step should have a driving force of ~300 mV (39). The second IET step of the proposed catalytic cycle (IET 2) occurs after transfer of an electron to exogenous cyt *c*. Thus, in the forward reaction of the overall catalytic cycle, the IET 2 step is initiated from the *one-electron reduced* Mo(V)/Fe(III) state of the enzyme, and both the sulfite and cyt *c* substrates are present. In contrast, the laser flash photolysis determination of IET 2 starts with the fully oxidized resting state (Mo(VI)/Fe(III)) of the enzyme and no substrates are present. One-electron photoreduction of this oxidized resting state species gives Mo(VI)/Fe(II), and the postulated conformational equilibria of this one-electron reduced state enables IET 2 to be observed in the forward and reverse directions (eq. 5) (13). The R309 and H304 mutations that show large decreases in IET 2 rates (Figure 5) but high k_{cat} values (Figure 4A) may reflect unfavorable resting state conformations of the fully oxidized enzymes, slow motional dynamics for bringing the heme and molybdenum domains into close proximity for the IET 2 reaction after photoreduction, or altered Mo(VI/V) potentials that make k_f (eq. 5) thermodynamically unfavorable in the flash photolysis experiments. The reduction potentials of the metal centers are discussed in the following section.

Spectroelectrochemistry and IET equilibrium constants

H304 and R309 are located in the Mo domain, and it seems reasonable to suppose that unless the heme domain comes within close proximity of them during the IET conformational change, these residues should not influence the heme midpoint potential because of their large distance from the iron. Due to a limited supply of protein, spectroelectrochemistry could not be performed on two mutant hSO enzymes, H304A and R309E. However, the remaining mutations showed a variety of effects on the heme midpoint potential.

The H304E, H304R, and H304R/R309H had heme potentials similar to that of wt hSO (54 mV). H304F hSO showed the largest change of the H304 mutations with an 11 mV negative shift. Overall, however, the H304 mutations had only small effects on the heme midpoint potential.

Two R309 mutations, R309K and R309M, caused significant decreases in the heme midpoint potential, with changes of −31 mV and −24 mV, respectively. In contrast, R309H hSO had a heme potential close to that of wt.

The spectroelectrochemistry results suggest that the heme domain interacts with the surface of the Mo domain near H304 and R309. This is supported by the changes in heme midpoint potential of R309M, R309K, and H304F and the dramatic changes in their IET 2 rates. The docking position of the heme during IET 2 is still unknown, but it has been proposed that the negatively charged heme domain interacts with the positively charged active site, possibly hydrogen bonding to active site residue R160 (40). During catalysis, however, having sulfite binding and sulfate release happening almost simultaneously with the heme domain docking may be unfavorable. An alternative model is that the heme docks in another location on the surface of the Mo domain that is close to the active site (18), such as the H304R, R309 area. Under this hypothesis the IET 2 rates and the heme potential would be altered if this interaction were disrupted by mutation of H304 or R309.

The potentials for the Mo center cannot be measured directly by spectroelectrochemistry, which is dominated by the absorbance of the heme. Insufficient amounts of the mutant proteins were available to measure the Mo potentials by EPR titrations. However, the Mo(VI/V) potentials can be calculated from the IET equilibrium constants from the flash photolysis experiments (eqs. 5, 10) provided that the Mo:Fe ratio is ~1:1. For the H304 mutants the ICP analyses (Table S1) showed that the Mo to Fe ratio was ~0.6; therefore, meaningful Mo potentials could not be calculated for these mutants. However, for the R309 mutants the Mo to Fe ratios determined by ICP (Table S1) were sufficiently large that the IET equilibrium constants could be used to calculate the Mo(VI/V) potentials (Table 2). None of the R309 mutations dramatically changed the Mo potential as compared to wt (Table 2). Thus, although the heme midpoint potentials for R309M and R309K are significantly lower than wt, the fact that the K_{eq} values are shifted to a value closer to one, reflects the smaller driving force between Fe and Mo for these two mutants.

Fatal mutation R309H

Several fatal point mutations have been identified in patients diagnosed with sulfite oxidase deficiency, including R309H (10). This work shows that purified R309H hSO has substantially *increased* catalytic activity (~3-fold greater than wt) and a slightly less efficient K_m sulfite. At pH 7.6, k_{et} is ~2 $k_{turnover}$, so as noted above, IET 2 is not rate limiting. This mutation gave small positive changes in the midpoint potentials (Table 2) of the heme (+7 mV) and Mo (+11 mV) that are marginally significant.

Unlike other fatal hSO mutations that have been studied (22, 25, 26), the data for purified R309H do not reveal any obvious reasons for this mutation causing sulfite oxidase deficiency. The midpoint potentials of Fe and Mo are somewhat increased, $K_m^{sulfite}$ is slightly increased, the activity is increased, and the enzyme still shows IET, although the rates are slow compared to wt. It is possible that these combined slight changes of the properties of the protein could cause SO deficiency; however, attractive alternative explanations are that this mutation causes structural instability or expression problems *in vivo*.

Conclusions

The catalytic cycle of Figure 1 has been the standard model for describing and analyzing the mechanism of vertebrate SOs, including hSO, for over 30 years (1, 4). The catalytic mechanism of SO includes two redox active metals (Mo(VI/V/IV) and Fe(III/II)), and two substrates (sulfite and cyt *c*). A previous detailed kinetic study of native chicken SO (cSO) investigated the steady-state reduction of sulfite by cyt *c*, as well as the kinetics of the rapid reduction of cSO by sulfite in the absence of cyt *c* (29). The rapid two-electron reduction by sulfite generated substantial amounts of the Fe(II)/Mo(V) state of SO (Figure 1), consistent with microcoulometic studies of cSO which yield a driving force of ~300 mV for the IET 1 process (39). The reaction of oxidized SO with excess sulfite is also an efficient method for generating the Mo(V) state for detailed structural studies by pulsed EPR spectroscopy (41).

The proposed oxidative half-reaction of hSO (left side of Figure 1) involves two one-electron *intermolecular* steps with an intervening *intramolecular* electron transfer reaction (IET 2). The one-electron reduced Fe(II)/Mo(VI) state of hSO can be produced directly in the absence of substrates by laser flash photolysis, and the kinetics of *intramolecular* electron transfer (IET 2) followed spectrophotometrically (Figure 5) (38). In spite of the small driving force for the IET 2 reaction (39, 17) and the 32 Å distance between Fe and Mo in the cSO crystal structure (11), k_{et} is much larger than $k_{turnover}$ for wt cSO and hSO. This observation led to the proposal that facile interdomain motion of the Fe(II)/Mo(VI) state decreases the Fe...Mo distance and facilitates rapid intramolecluar electron transfer (IET 2) (13). The kinetic and thermodynamic properties of numerous mutants of recombinant hSO have been investigated to gain additional insight into the proposed overall mechanism of hSO (Figure 1), the interdomain motion model for IET 2, and clues why certain mutations cause isolated sulfite oxidase deficiency. The present work shows that the H304 and R309 mutants of hSO all have *smaller* k_{et} values than wt hSO, but that their k_{cat} values are *greater* than wt hSO. However, in nearly all cases the value of k_{et} is substantially greater than $k_{turnover} = 1/2k_{cat}$ (see Table S3). Even the R309E mutant that reverses the charge at residue

309 from positive to negative, has $k_{tunover} < k_{et}$. Thus, for these H304 and R309 mutants, as with wt hSO, IET 2 is not the rate limiting step. In contrast, several catalytically competent mutants of R472 (42) and of aromatic surface residues of the Mo domain (18) show greatly impaired IET 2 ($k_{et} << k_{turnover}$). Clearly, crystal structures of some of these mutants of hSO are important for understanding their detailed conformations and properties. However, to date only one crystal structure of an *intact* SO protein is available, that of native cSO (11), and recombinant hSO proteins have proven to be unusually difficult to crystallize in their intact form. Theoretical studies of the dynamics of interdomain motion have begun to appear (15, 16) that corroborate the proposal from the viscosity dependence of the rate of IET 2 for wt SO (14), but direct experimental measurements of the proposed interdomain dynamics are not yet available. Thus, complete unraveling of the intimate mechanism of hSO and the reasons that certain mutations are fatal remains an unresolved challenge.

Finally, the kinetic and spectroscopic properties of a purified mutant protein may not indicate why the particular mutation is fatal *in vivo*. For example, although the exact role of the phosphate group of Moco in hSO is not known, the surrounding network of hydrogen bonding residues could possibly protect the cofactor from degradation by the action of phosphatases within the cell. *In vitro* studies of purified mutant proteins eliminate interactions with other enzymes and bioactive molecules, and under such conditions some hSO mutants might exhibit enhanced steady-state activity.

Supplementary Material

Refer to Web version on PubMed Central for supplementary material.

Acknowledgements

Support of this research by the National Institute of General Medical Sciences is gratefully acknowledged (Grant GM-37773 to JHE; Ruth L. Kirchstein-NIH Fellowship1F32GM082136-01 to KJW). We thank Dr. K. V. Rajagopalan for providing the pTG918 plasmid containing the hSO gene used to prepare the recombinant hSO enzyme. We thank Dr. F. Ann Walker for the use of equipment and Dr. R. E. Berry for helpful discussions. A.C.D. was a participant in the Undergraduate Biology Research Program and was supported in part by a grant to the University of Arizona from the Howard Hughes Medical Institute (52003749).

References

1. Rajagopalan, KV. Sulfite Oxidase (Sulfite:Ferricytochrome c Oxidoreductase).. In: Coughlan, MP., editor. Molybdenum and Molybdenum-Containing Enzymes. 1st ed.. Pergamon Press; Oxford, U.K.: 1980. p. 241-272.
2. Johnson JL, Rajagopalan KV. J. Biol. Chem. 1977; 252:2017–2025. [PubMed: 14956]
3. Kessler DL, Rajagopalan KV. J. Biol. Chem. 1972; 247:6566–6573. [PubMed: 4342603]
4. Hille R. Biochim. Biophys. Acta. 1994; 1184:143–169. [PubMed: 8130250]
5. Cohen HJ, Betcher-Lange S, Kessler DL, Rajagopalan KV. J. Biol. Chem. 1972; 247:7759–7766. [PubMed: 4344230]
6. Schindelin H, Kisker C, Rajagopalan KV. Adv. Protein. Chem. 2001; 58:47–94. [PubMed: 11665493]
7. Schwarz G, Mendel RR. Annu. Rev. Plant Biol. 2006; 57:623–647. [PubMed: 16669776]
8. Veldman A, Santamaria-Araujo JA, Sollazzo S, Pitt J, Gianello R, Yaplito-Lee J, Wong F, Ramsden CA, Reiss J, Cook I, Fairweather J, Schwarz G. Pediatrics. 2010; 125:e1249–1254. [PubMed: 20385644]

9. Rupar CA, Gillett J, Gordon BA, Ramsay DA, Johnson JL, Garrett RM, Rajagopalan KV, Jung JH, Bacheyie GS, Sellers AR. Neuropediatrics. 1996; 27:299–304. [PubMed: 9050047]
10. Johnson JL, Coyne KE, Garrett RM, Zabot MT, Dorche C, Kisker C, Rajagopalan KV. Hum. Mutat. 2002; 20:74. [PubMed: 12112661]
11. Kisker C, Schindelin H, Pacheco A, Wehbi WA, Garrett RM, Rajagopalan KV, Enemark JH, Rees DC. Cell. 1997; 91:973–983. [PubMed: 9428520]
12. Astashkin AV, Rajapakshe A, Cornelison MJ, Johnson-Winters K, Enemark JH. J. Phys. Chem. B. 2012; 116:1942–1950. [PubMed: 22229742]
13. Pacheco A, Hazzard JT, Tollin G, Enemark JH. J. Biol. Inorg. Chem. 1999; 4:390–401. [PubMed: 10555573]
14. Feng C, Kedia RV, Hazzard JT, Hurley JK, Tollin G, Enemark JH. Biochemistry. 2002; 41:5816–5821. [PubMed: 11980485]
15. Pushie MJ, George GN. J. Phys. Chem. B. 2010; 114:3266–3275. [PubMed: 20158265]
16. Utesch T, Mroginski MA. J. Phys. Chem. Lett. 2010; 1:2159–2164.
17. Johnson-Winters K, Nordstrom AR, Emesh S, Astashkin AV, Rajapakshe A, Berry RE, Tollin G, Enemark JH. Biochemistry. 2010; 49:1290–1296. [PubMed: 20063894]
18. Rajapakshe A, Meyers KT, Berry RE, Tollin G, Enemark JH. J. Biol. Inorg. Chem. 2012; 17:345–352. [PubMed: 22057690]
19. Davis AC, Cornelison MJ, Meyers KT, Rajapakshe A, Berry RE, Tollin G, Enemark JH. Dalton Trans. 2013; 42:3043–9. [PubMed: 22975842]
20. Wilson HL, Rajagopalan KV. J. Biol. Chem. 2004; 279:15105–15113. [PubMed: 14729666]
21. Feng C, Wilson HL, Hurley JK, Hazzard JT, Tollin G, Rajagopalan KV, Enemark JH. J. Biol. Chem. 2003; 278:2913–2920. [PubMed: 12424234]
22. Feng C, Wilson HL, Hurley JK, Hazzard JT, Tollin G, Rajagopalan KV, Enemark JH. Biochemistry. 2003; 42:12235–12242. [PubMed: 14567685]
23. Feng C, Wilson HL, Tollin G, Astashkin AV, Hazzard JT, Rajagopalan KV, Enemark JH. Biochemistry. 2005; 44:13734–13743. [PubMed: 16229463]
24. Astashkin AV, Johnson-Winters K, Klein EL, Feng C, Wilson HL, Rajagopalan KV, Raitsimring AM, Enemark JH. J. Am. Chem. Soc. 2008; 130:8471–8480. [PubMed: 18529001]
25. Rajapakshe A, Tollin G, Enemark JH. Chem. Biodiversity. 2012; 9:1621–1634. doi:10.1002/cbdv.201200010.
26. Emesh S, Rapson TD, Rajapakshe A, Kappler U, Bernhardt PV, Tollin G, Enemark JH. Biochemistry. 2009; 48:2156–2163. [PubMed: 19226119]
27. Temple CA, Graf TN, Rajagopalan KV. Arch. Biochem. Biophys. 2000; 383:281–287. [PubMed: 11185564]
28. Garrett RM, Rajagopalan KV. J. Biol. Chem. 1996; 271:7387–7391. [PubMed: 8631762]
29. Brody MS, Hille R. Biochemistry. 1999; 38:6668–6677. [PubMed: 10350486]
30. Kipke CA, Cusanovich MA, Tollin G, Sunde RA, Enemark JH. Biochemistry. 1988; 27:2918–2926. [PubMed: 3401455]
31. Hurley JK, Weber-Main AM, Stankovich MT, Benning MM, Thoden JB, Vanhooke JL, Holden HM, Chae YK, Xia B, Cheng H, Markley JL, Martinez-Julvez M, Gomez-Moreno C, Schmeits JL, Tollin G. Biochemistry. 1997; 36:11100–11117. [PubMed: 9287153]
32. Tollin, G. Interprotein and Intraprotein Electron Transfer Mechanisms. In: Balzani, V., editor. Electron Transfer in Chemistry. Vol. IV. Wiley-VCH Verlag GmbH; Weinheim, Germany: 2008. p. 202-231.
33. Tollin G. J. Bioenerg. Biomembr. 1995; 27:303–309. [PubMed: 8847344]
34. Tollin G, Hurley JK, Hazzard JT, Meyer TE. Biophys. Chem. 1993; 48:259–279. [PubMed: 8298059]
35. Berry RE, Shokhireva T, Filippov I, Shokhirev MN, Zhang H, Walker FA. Biochemistry. 2007; 46:6830–6843. [PubMed: 17506528]
36. Ding XD, Weichsel A, Andersen JF, Shokhireva TK, Balfour C, Pierik AJ, Averill BA, Montfort WR, Walker FA. J. Am. Chem. Soc. 1999; 121:128–138.

37. Hellwig P, Behr J, Ostermeier C, Richter OM, Pfitzner U, Odenwald A, Ludwig B, Michel H, Mantele W. Biochemistry. 1998; 37:7390–7399. [PubMed: 9585553]
38. Feng C, Tollin G, Enemark JH. Biochim. Biophys. Acta. 2007; 1774:527–539. [PubMed: 17459792]
39. Spence JT, Kipke CA, Enemark JH, Sunde RA. Inorg. Chem. 1991; 30:3011–3015.
40. Kappler U, Bailey S. J. Biol. Chem. 2005; 280:24999–25007. [PubMed: 15863498]
41. Klein EL, Astashkin AV, Raitsimring AM, Enemark JH. Coord. Chem. Rev. 2013; 257:110–118. [PubMed: 23440026]
42. Johnson-Winters K, Davis AC, Arnold AR, Berry RE, Tollin G, Enemark JH. J. Biol. Inorg. Chem. 2013; 18:645–653. [PubMed: 23779234]

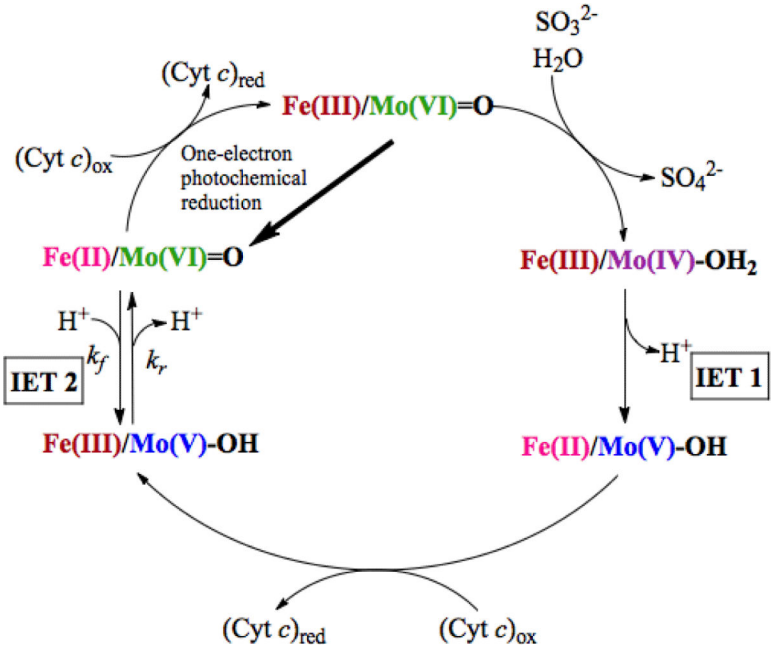

Figure 1.

Proposed oxidation state changes occurring at the Mo and Fe centers of one subunit of hSO during the catalytic oxidation of sulfite and the concomitant reduction of (cyt c)$_{ox}$. Only the equatorial oxygen atom among the ligands of Mo is shown for clarity. The one-electron photochemical reduction of Fe(III), indicated by the solid dark arrow, generates the Fe(II)/Mo(VI) state which undergoes IET 2. The directions of k_f and k_r refer to the flash photolysis experiment. Adapted from (19).

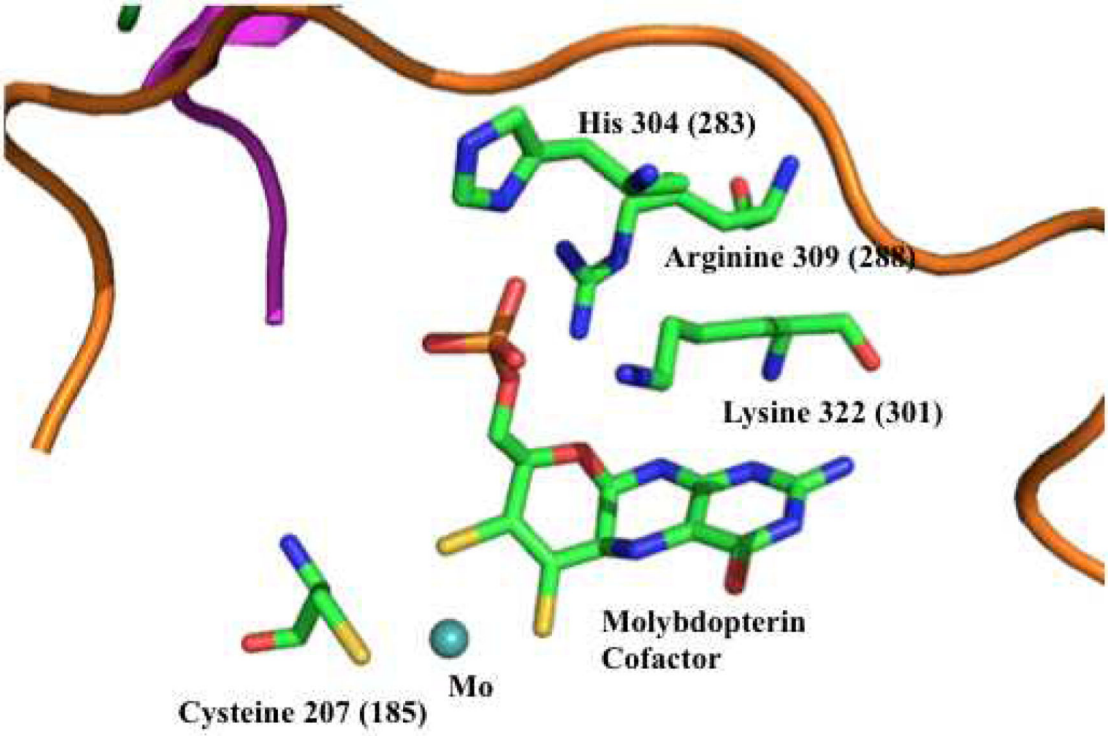

Figure 2.

Crystal structure of cSO[11] (pdb 1SOX) showing H304, R309, K322, C207 and the molybdenum cofactor. Numbering reflects hSO, while cSO numbering is shown in parenthesis.

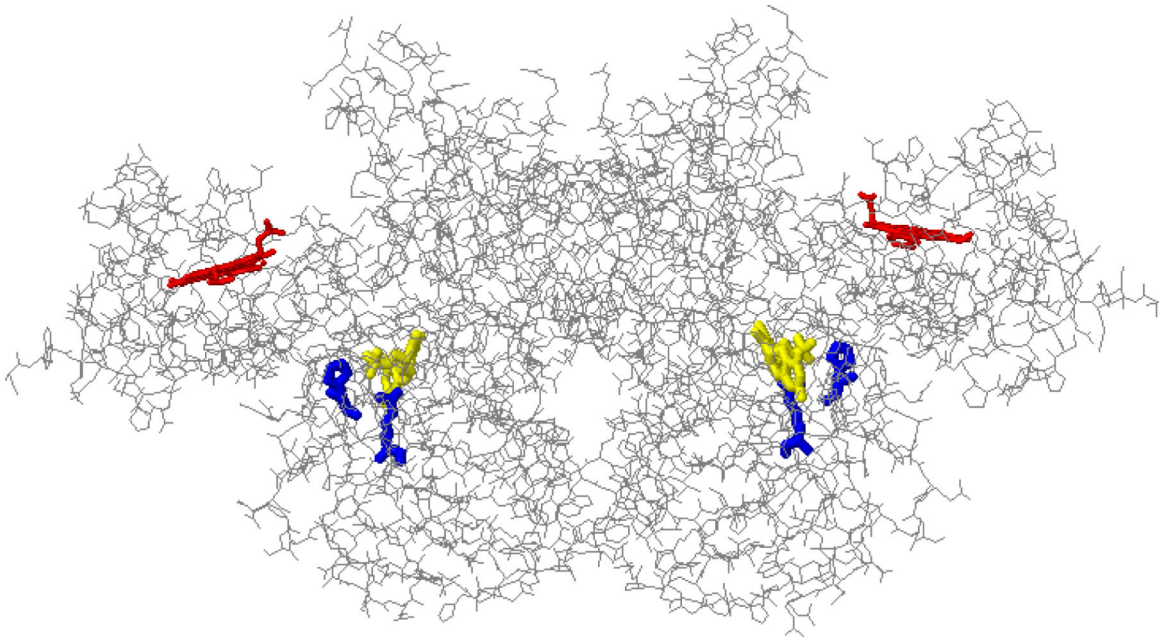

Figure 3.
Crystal structure of cSO[11] (pdb 1SOX). Heme shown in red, Moco shown in yellow, and residues that have been mutated in hSO are in blue.

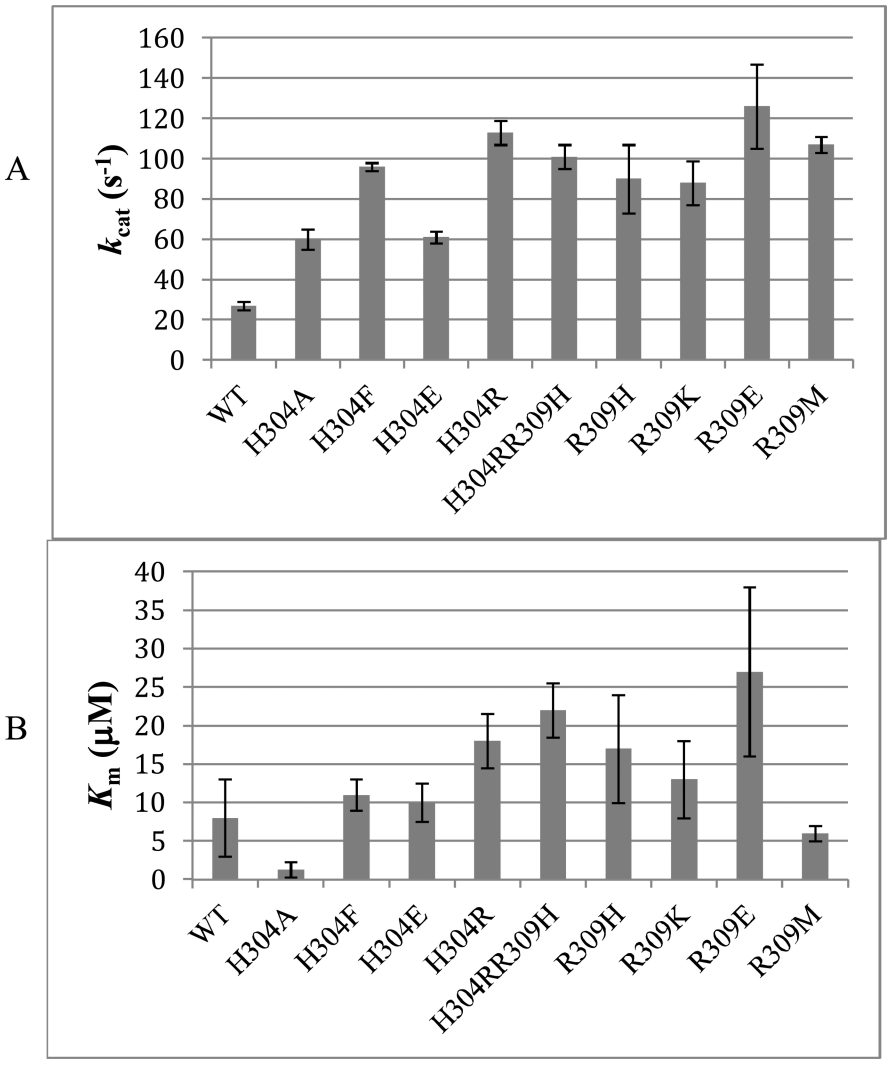

Figure 4.

The k_{cat} (A) and K_m (B) values for H304 and R309 mutants compared to wt hSO, measured using 20 mM Tris Acetate, pH 7.6

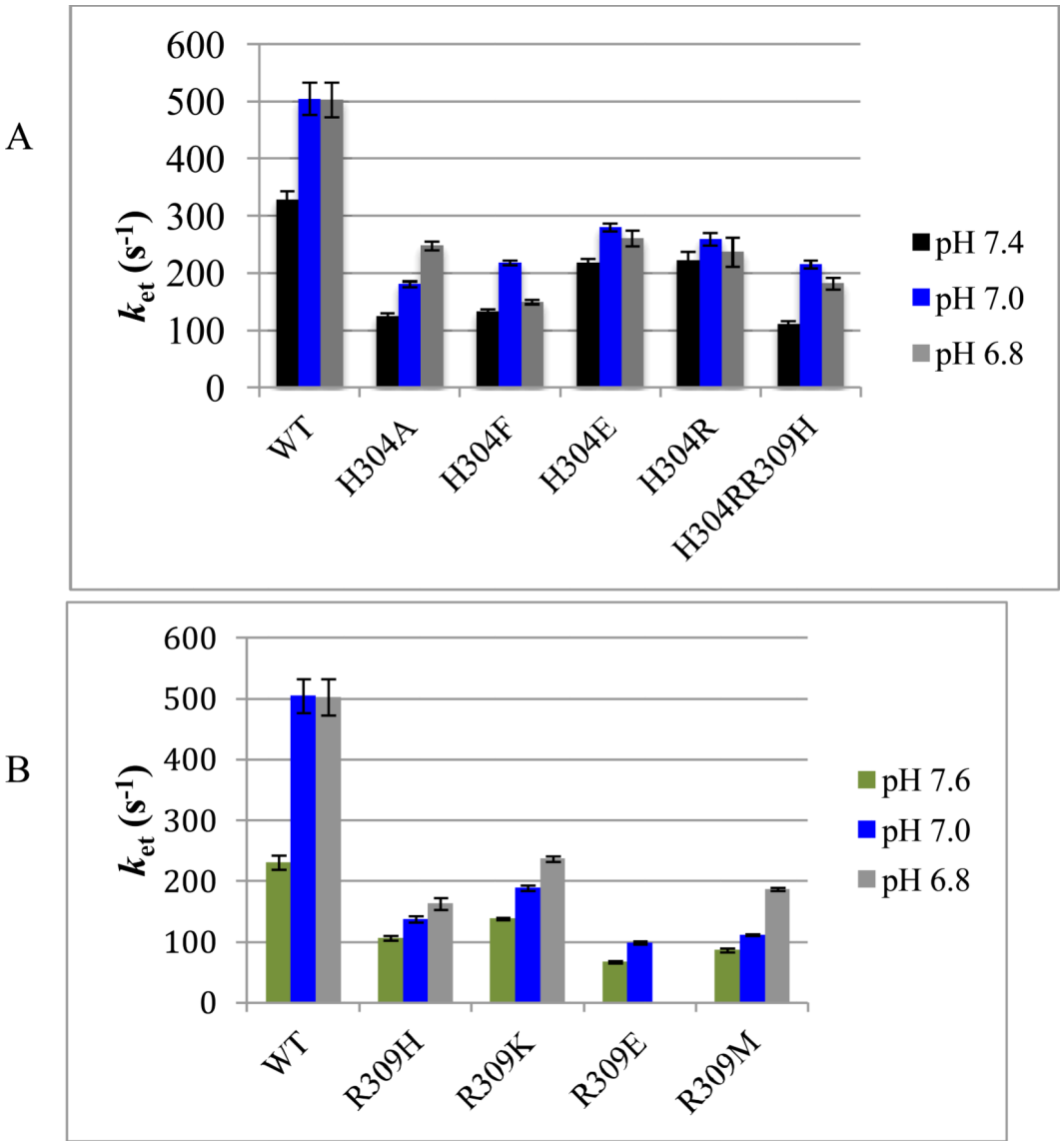

Figure 5.
IET rates ($k_{et}(s^{-1})$) for the H304 (A) and R309 (B) mutants, measured using 20 mM Tris Acetate.

Table 1

The Fe midpoint potentials of H304 mutants versus wt hSO, measured using 20 mM Tris Acetate at pH 7.4

	Fe midpoint potential (mV vs SHE)
wt	**54 ± 2**
H304F	43 ± 2
H304E	56 ± 2
H304R	51 ± 2
H304R/R309H	52 ± 2

Table 2

The Fe midpoint potentials, IET K_{eq} values, and calculated Mo midpoint potentials of R309 mutants versus wt hSO, measured using 20 mM Tris Acetate at pH 7.4

	Fe midpoint potential (mV vs SHE)	K_{eq}	Calculated Mo potential (mV vs SHE)
wt	**54 ± 2**	**0.36** ± 0.01	**27**
R309H	61 ± 3	0.41 ± 0.02	38
R309K	23 ± 5	1.24 ± 0.04	29
R309M	30 ± 5	0.79 ± 0.05	24